Complete bandgap switching in photonic opals

New Journal of Physics
The open-access journal for physics

Complete bandgap switching in photonic opals

D P Aryal, K L Tsakmakidis and O Hess[1]
Advanced Technology Institute and Department of Physics,
Faculty of Engineering and Physical Sciences, University of Surrey,
Guildford GU2 7XH, UK
E-mail: o.hess@surrey.ac.uk

New Journal of Physics **11** (2009) 073011 (14pp)
Received 25 January 2009
Published 3 July 2009
Online at http://www.njp.org/
doi:10.1088/1367-2630/11/7/073011

Abstract. A comprehensive theoretical study of the optical properties and switching competence of double-shell photonic crystals (DSPC) and double-inverse-opal photonic crystals (DIOPC) is presented. Our analysis reveals that a DIOPC structure with a silicon (Si) background exhibits a complete photonic bandgap (PBG), which can be *completely* switched on and off by moving the core spheres inside the air pores of the inverse opal. We show that the size of this switchable PBG assumes a value of 3.78% upon judicious structural optimization, while its existence is almost independent of the radii of the interconnecting cylinders, whose sizes are difficult to control during the fabrication process. The Si-based DIOPC may thus offer a novel and practical route to *complete* PBG switching and optical functionality.

Contents

[1] Author to whom any correspondence should be addressed.

1. Introduction

Controlling the flow of light is one of the major challenges in modern optics. With optical telecommunication and computing technologies becoming increasingly important, there is an ever-growing need for devices that will be able to control and manipulate lightwave signals. Classic means for controlling light signals are Bragg mirrors, waveguides, resonators, and beam splitters. However, considering that the diversity of modern optical devices has dramatically increased, there are nowadays a plethora of new challenges in our quest for new ways to manipulate light. An example of desired materials-based functionality is structural color (iridescent, prismatic, multihued or luminescent), which allows for avoiding the environmentally unfriendly traditional dies, and being built of components that are benign while being universally attractive in competitive marketplaces, such as mobile electronics and the automotive or airline industries [1]–[6]. Further applications include windows whose appearance can be changed on demand (e.g. from opaque to transparent and vice versa) or windows that adapt their transmission properties to the direction of incident light, e.g. for more efficient solar panels [7]. It is clear that such kinds of applications fundamentally entail an exploration and pursuit of new ideas, designs and photonic devices that will enable us to mold the flow of light beyond current constraints.

Photonic crystals (PCs) are engineered structures that allow for just such a photonic functionality on the materials level, enabling the complete prohibition or allowance of the propagation of light in certain directions and at certain frequencies [8, 9]. PCs are, in this regard, highly attractive because they allow the design and manipulation of their photonic properties based on the so-called 'band-structure engineering'. For the aforementioned applications, opal-based PCs are the most promising candidates, since they possess three-dimensional (3D) photonic properties, and can simultaneously be fabricated on large scales and at low cost [10]–[12]. A further attraction of these structures lies in the possibility of dynamically (actively) tuning their optical properties, which may allow for the realization of controllable and functional nanophotonic devices.

Since the photonic band structure mainly depends on the spatial (geometric) arrangement of the crystal and the refractive indices of the constituent materials, there are currently two main approaches to tunable PBGs. The first approach is based on changing the lattice constants or the spatial symmetry by means of external forces, such as mechanical forces [13]–[15], electrical/magnetic fields [16] or light [17]. Although large shifts in the existing photonic bandgaps (PBGs) have been demonstrated with these techniques, the required structural changes, which are of the order of micrometer dimensions, may limit the practical deployment of such schemes in certain nanophotonic applications. The second of the aforesaid methodologies is based on controlling the refractive indices of the materials. Liquid crystals have been widely used for this purpose, particularly because of the considerable variation of their optical properties [18]–[22]. Besides, the refractive indices of semiconductor PC materials can also be tuned using free carrier injection and/or photoexcitation [23]–[27]. While promising and interesting results have been experimentally demonstrated (e.g. ultrafast optical switching), these approaches have not yet, to our knowledge, resulted in complete PBG switching.

However, a number of new and more challenging applications, such as structural color or switchable windows that we mentioned above, require tunable structures that can allow for a *complete* switching of the PBG. Further, such applications include the dynamic control of the density of states (DOS) and the photonic spontaneous emission [27, 28] inside PBG cavities.

While spontaneous emission switching relies critically on changes in the local DOS, which can be achieved in conventional inverse opals [28] without requiring complete switching of the PBG, clearly the ability to close a PBG and open it over *all* angles (complete PBG) is the only means for completely trapping photons inside PC cavities. Completely capturing and releasing photons held within PC cavities will also be beneficial for recently introduced PC-based approaches for stopping and storing light [29]. To address these challenges, here we make use of a new class of recently experimentally realized [11, 12] inverse-opal PCs, wherein each air void of a conventional inverse opal is replaced by a hybrid sphere made of a core and a shell region of different materials. As will be shown in detail in the following, such PC arrangements open up new perspectives for achieving a *complete* switching of the PBG.

It is the objective of the present work to introduce and explore novel, 3D, inverse-opal-based PC designs that allow for completely switching on and off a 3D PBG. The paper is organized as follows. We begin by introducing and studying two novel PC designs, namely an inverse opal with core (air) spheres surrounded by a dielectric shell (SiO_2), which we call a double-shell photonic crystal (DSPC), and an inverse opal of spherical air pores, interconnected via air channels and with movable dielectric (SiO_2) core spheres inside the air pores, which we call a double-inverse-opal photonic crystal (DIOPC) [11, 29, 30]. For low-index contrast, titania-based designs [31], we show that both PC structures possess photonic stopgaps, the dependence of which on the variation of the optogeometric parameters is investigated in detail. We then study a silicon-based ($n_{Si} = 3.736$) DIOPC structure, having titania spherical scatterers inside its air pores, and we show that the complete PBG possessed by this configuration can be switched on and off by moving the TiO_2 scatterers in different directions. We also explain how this switching process, occurring in a DIOPC structure that has previously been experimentally realized [11, 12], can be accomplished in a future experiment. Finally, we conclude with a summary of the presented results.

2. Partial PBGs in DSPC and DIOPC structures

The structure of a face-centered-cubic (fcc) close-packed lattice and its corresponding first Brillouin zone are, respectively, illustrated in figures 1(a) and (b), where the open circles indicate the high symmetry points Γ, L, X, U, W and K. The points L, X, and K correspond to the (111), (100) and (110) directions, respectively. In particular, the (111) direction is of prime interest here, since it corresponds to the growth direction of the PC and is therefore the most convenient direction for optical measurements.

Figure 1(c) schematically illustrates a DSPC. Each sphere in the inverse-opal periodic structure is composed of a core, along with an accompanying shell that is made of a different dielectric material; the resulting structure is embedded in a high-index dielectric background. In this work, we shall confine our discussions to DSPCs having a hollow core ($n_c = 1$) of radius R_p. Let us, further, assume that the spherical shell is made of silica ($n_{sp} = n_{SiO_2} = 1.5$) and has external radius R_{sp}. We choose the background dielectric to be titania ($n_b = n_{TiO_2} = 2.5$) because this material exhibits low absorption in the visible regime, and its infiltration leads to a less porous material; it can, thus, constitute a good candidate background material for the herein envisaged PC applications, particularly in relation to (semi-) transparent panels in the visible regime.

In figure 2(a), we plot the 3D dielectric distribution of a DIOPC structure, whereas figures 2(b)–(d) schematically illustrate the movement of the silica (red) core spheres from

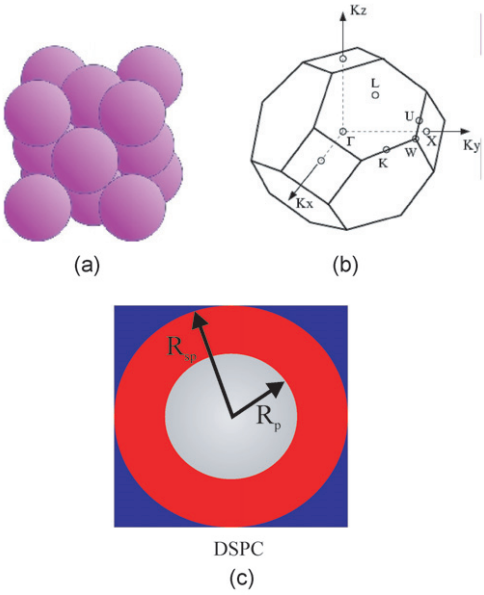

Figure 1. (a) Schematic representation of an fcc structure. (b) The corresponding first Brillouin zone of the fcc lattice. The point Γ indicates the centre of the first Brillouin zone, while K, L, X, U and W are the high-symmetry points on the edges of the Brillouin zone. (c) Illustration of a unit cell of the DSPC structures, along with the associated geometric definitions.

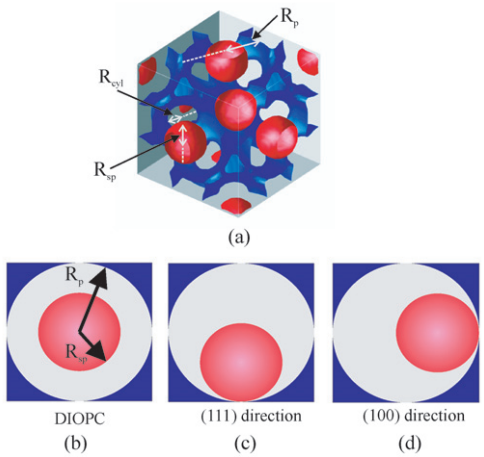

Figure 2. (a) Illustration of an eight-unit-cell DIOPC structure, along with its associated geometric definitions. (b)–(d) Schematic representation of the DIOPC bandgap switching by movement of the core spheres (red) in different directions. In (c) and (d), the core spheres are tangential to the background dielectric (blue).

their 'natural' (111) position (in the absence of any external force but gravity) toward the (100) direction, used in the switching process. The silica spheres may have small metallic cores (not shown in figure 2) allowing for their collective movement in the desired direction by application of external magnetic or electric fields [29] (see also section 3). The air pores have radius R_p and

are either simply embedded in the background material or are interconnected via cylindrical channels of radius R_{cyl}, as shown in figure 2(a).

Like in the DSPC structure, we here assume that the background material is titania. The principle of the fabrication process and experimental demonstration of such structures have been detailed in a series of recent works [11, 12]. Similarly to standard inverse opal PCs [10, 32, 33], fabricated DIOPC structures possess excellent uniformity and are well ordered, with their geometric parameters being adjusted precisely during the fabrication process [11, 12]—an essential requirement for the manifestation of complete 3D PBGs [34]. The DIOPC structure studied in this section does not contain interconnecting cylinders (of radius R_{cyl}, shown in figure 2(a)), i.e. the air pores are not connected by air cylinders, but are only closely packed and, occasionally, overlapping.

The optical properties of the aforementioned structures have been simulated using *ab initio* band structure calculations, on the basis of high-accuracy plane-wave expansions of the magnetic field components on a reciprocal lattice, combined with appropriate periodic boundary conditions [35]. It is to be noted that the shifting of the spheres from their central position in the DIOPC structure breaks some symmetries of the fcc lattice; hence, some high-symmetry points, shown in figure 1(b), are not equivalent any more. This effect is taken into account in the presented simulations when determining the position of the stopgaps.

The band structure of the DSPC for $R_p = 0.25a$ and $R_{sp} = 0.354a$, with a being the (fcc) lattice constant of the crystal, is illustrated in figure 3(a). One may notice from this figure that the dielectric contrast is lower than the one required for a complete PBG to appear. Nonetheless, this DSPC structure does exhibit two stopgaps between the 2nd and the 3rd band, at the L and X points, respectively.

The gap/mid-gap ratio (GMR) between the 2nd and the 3rd band at the L point is found to be 16.78%, with a mid-gap frequency of 0.51. Similarly, the GMR at the X point between the 2nd and the 3rd band is found to be 1.96%. In figure 3(b), we present the corresponding band structure of the DIOPC for $R_{sp} = 0.25a$ and $R_p = 0.354a$. From this dispersion diagram one may readily observe that there is a stopgap between the 2nd and 3rd bands, at points L and X, respectively. The magnitude of the GMR at the L point is found to be 13.4%, having a mid-gap frequency of 0.56, and is indeed smaller than the corresponding one occurring in the case of the DSPC structure.

It is valid and interesting to investigate the potential for tuning the stopgaps in both of the aforementioned structures. To this end, figure 4(a) shows the variations of the stopgaps in the DSPC with the inverse-opal sphere radius, R_{sp}. For this case, a pore radius of $R_p = 0.25a$ is chosen. Note that an increase in the radius R_{sp} above $0.354a$ forces the spheres to overlap. It is also interesting to realize that in the limiting case for which $R_{sp} = 0.5a$, the DSPC structure becomes similar to an inverse opal of air spheres with radius $0.25a$ having silica background. The other limiting case, $R_{sp} = 0.5a$, corresponds to an inverse opal of air spheres with radius $0.25a$ in a titania background. We observe from figure 4(a) that the GMR at the L point assumes a maximum value of 17.34% for $R_p/R_{sp} = 0.735$. The GMR at the X point, on the other hand, becomes maximum (7%) for the aforementioned degenerate case, at which $R_p/R_{sp} = 1.0$ ($R_p = 0.25a$). Figure 4(b) displays the dependence on the air pore radius R_p of the stopgaps at points L and X of the DIOPC structure. Here, we again vary the radius of the air pore sphere R_p between the two limiting cases, namely $R_p = 0.25a$, which corresponds to an inverse opal of silica spheres in titania, and $R_p = 0.5a$, which corresponds to an opal structure made of silica spheres in air. We note that when the ratio R_{sp}/R_p varies between 0.5 and 0.625 the background

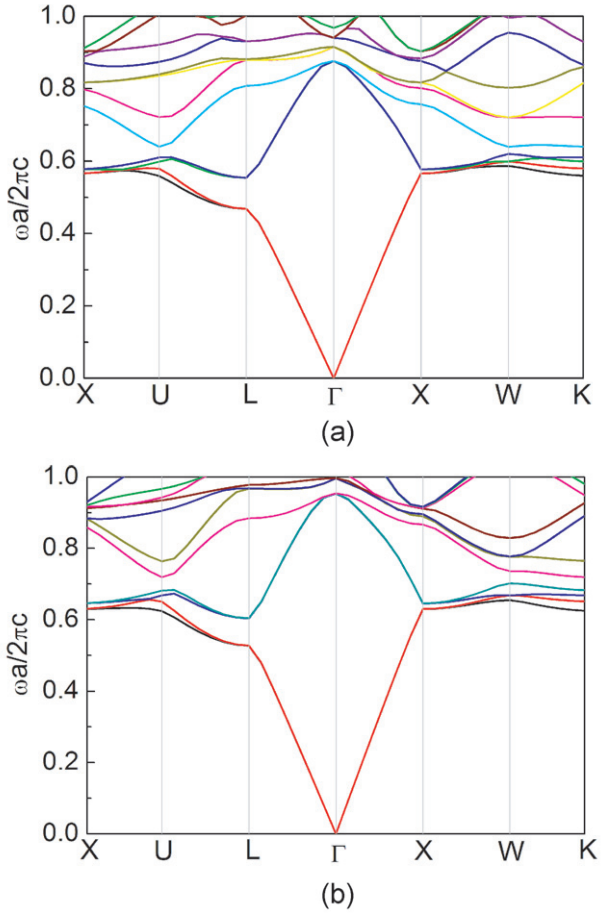

Figure 3. (a) Photonic band structure of a DSPC of close-packed silica spheres with hollow cores in a titania background with $R_p = 0.25a$ and $R_{sp} = 0.354a$. (b) Photonic band structure of a DIOPC of close-packed air pores and silica core spheres, embedded in titania, with $R_{sp} = 0.25a$ and $R_p = 0.354a$.

titania islands in the close-packed crystal are not connected and the resulting PC exhibits a transition from an opal to an inverse opal structure, evident in both curves of figure 4(b). Starting from $R_{sp}/R_p = 0.625$, the PC progressively assumes the behavior of an inverse opal. This can be further verified by means of the energy distributions within the constituents of the structure [29, 30].

Figures 5(a) and (b) summarize the influence of the core spheres' position and size on the stopgap between the 2nd and 3rd bands of the DIOPC at points L and X, respectively. The core spheres are positioned (within the air void) in three distinct ways, namely, centered cores and shifted cores along the (111) and (100) directions.

First, we note from figure 5(a) that for $R_{sp} < 0.05a$ the influence of the core spheres' radius on the GMR at point L appears to be constant (independent of the radius) for all three positions of the spheres. However, as the core radius increases, its influence on the GMRs in all three cases is found to be more pronounced. For the centered cores, as well as the ones shifted along the (100) direction, we observe a somewhat similar behavior in the evolution of the GMRs with the core radius, i.e. both GMRs decrease monotonically with increasing values of the radius.

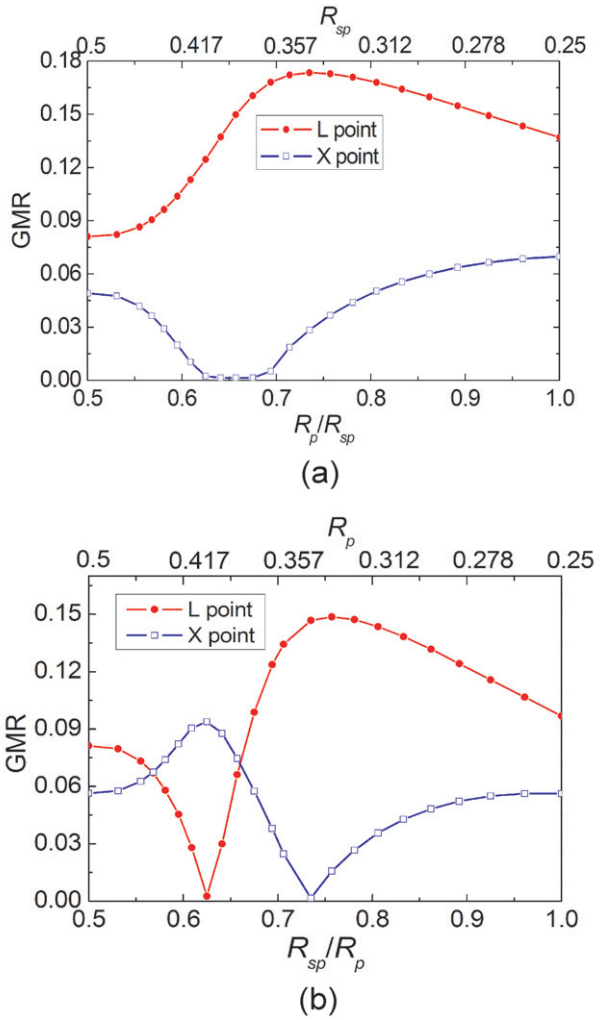

Figure 4. (a) Dependence of the GMR on $R_{\mathrm{p}}/R_{\mathrm{sp}}$ for a DSPC composed of hollow core and SiO_2 shell spheres ($n_{SiO_2} = 1.5$) in a titania background, with $R_{\mathrm{p}} = 0.25a$ and R_{sp} varying. (b) Dependence of the GMR on $R_{\mathrm{sp}}/R_{\mathrm{p}}$ for a DIOPC composed of air pores and SiO_2 core spheres ($n_{SiO_2} = 1.5$) in a titania background with $R_{\mathrm{sp}} = 0.25a$ and varying R_{p}.

In the case of core spheres shifted along the (111) direction, however, we observe a different behavior compared with the previous two cases. In this case, the GMR first increases with the core radius with the highest value of 19.9% for a core radius of $0.15a$, and afterwards it starts to decrease monotonically. Therefore, figure 5(a) indicates that the influence of the core spheres' position and radius on the stopgap for the (111)-shifting case is stronger compared with the other two cases. For a quantitative comparison of the GMR values in the above three different cases, let us focus on a core radius equal to $R_{\mathrm{sp}} = 0.15a$. We, then, immediately observe that the GMR value for spheres shifted along the (111) direction is 19.9%, which is larger than the one corresponding to the centered core spheres (17.03%) and the core spheres shifted along the (100) direction (17.86%). We may thus unambiguously conclude that the GMRs are more

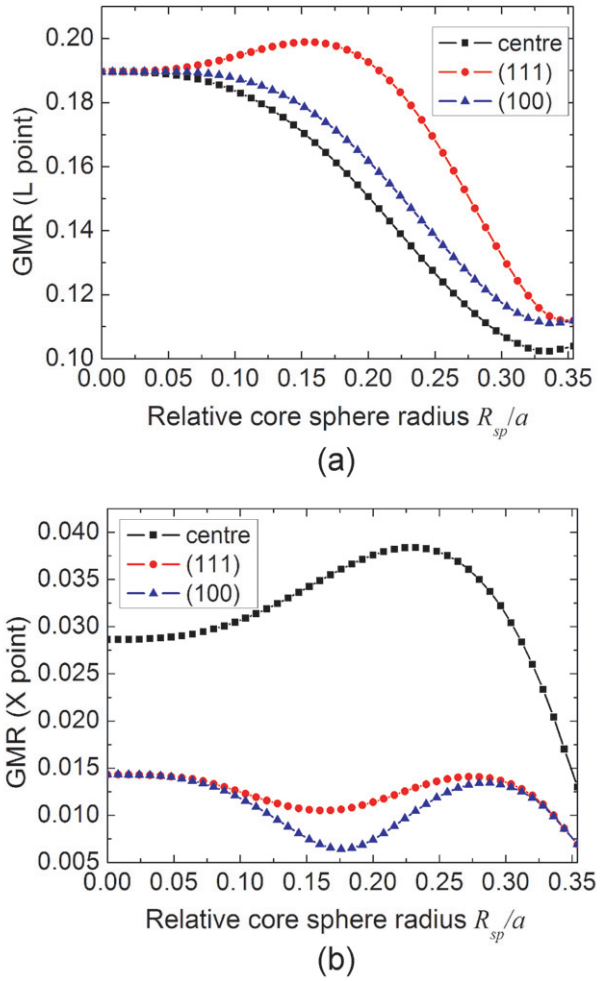

Figure 5. (a) Dependences on R_{sp} of the GMR between the 2nd and 3rd bands of the DIOPC at the (a) L point and (b) X point, when the silica core is centered, placed in its 'natural' (111) position or shifted along the (100) direction. Here, the silica core radius R_{sp} is varied, while the air pore radius is kept constant to $R_{\mathrm{p}} = 0.354a$ in a titania background. The cylinder radius is chosen to be $0.12a$.

influenced, i.e. more efficient switching is anticipated, when the core spheres are shifted to the (111) direction, i.e. back to their natural position inside the DIOPC in the absence of external fields, than in the centered or (100) directions.

The above conclusions change quite dramatically when we consider the GMR variations at the X point, as shown in figure 5(b). Unlike the previous case, we may now observe that, first, a similar behavior of the GMR dependences on the core radius occurs for the cases where the core spheres are shifted along the (111) and (100) directions. For core spheres shifted along the (111) direction, the GMR at X point decreases with an increase in core radius until it reaches its first smallest value (1.05%, for radius $R_{\mathrm{sp}} = 0.168a$). Its global minimum value of 0.69% is reached for a core sphere radius equal to $0.354a$. For the case where the core spheres are shifted along the (100) direction, we note that the GMR decreases monotonically for core sphere radii

$R_{sp} \leqslant 0.176a$. It becomes minimum (0.64%) for a core radius equal to $0.176a$. Afterwards, it starts to increase, reaching its second (global) highest value at around $R_{sp} = 0.27a$, beyond which it again decreases monotonically; finally, it assumes a value of 0.69%, for a core sphere radius exactly equal to $0.354a$.

The case that corresponds to the core spheres being centered is considerably different. Here, we find that the GMR increases with core sphere radius (for $R_{sp} \leqslant 0.23a$), assuming its global maximum value of 3.84% for a core radius of $R_{sp} = 0.23a$. For $R_{sp} \geqslant 0.23a$, the GMR values decrease monotonically. We thus arrive at a general and practical conclusion that for each core radius and at both the L and X points, the stopgaps of the DIOPC can be more efficiently switched when we move the core spheres from their natural (111) positions to the center of the inverse-opal air pores. Detailed simulations and evaluations of the 3D field distributions have additionally revealed that it is, indeed, the interaction between the field and the core spheres that appreciably influences the PBGs, especially when the core spheres are touching the background wall [30].

3. Switching of the complete PBG in an Si-based DIOPC

For applications concerning switchable windows that can be changed dynamically from completely opaque to completely transparent or for photonic functionality at telecommunication wavelengths, a stopgap may not be always sufficient. Therefore, in the following we will study the effects of the spheres' position in the case where a complete PBG can be obtained. Moreover, we aim to ascertain the existence of 'switching states', which correspond to completely opaque or completely transparent aspects, depending on the positioning of the spheres. In order to obtain a complete PBG of reasonable size, the index contrast in the structure should be increased. Therefore, in the following, we are considering DIOPC structures that have silicon as a background material ($n_b = n_{Si} = 3.736$). In principle, such Si-based PCs can also be integrated in optical circuits [36].

It is to be noted that the intensity loss (absorption) coefficient (g) of the intrinsic bulk Si for photon energies smaller than 1.7 eV ($\approx$729 nm) is smaller than approximately 0.009 [37]–[39], monotonically decreases with decreasing photon energies (at telecommunication wavelengths close to zero) and is not expected to fundamentally qualitatively alter the principal conclusions of our present studies—as long as one considers modes with *real* wavenumber and *complex frequency* [40]. For instance, even for wavelengths larger than 729 nm ($g = 1.6718 \times 10^3$ cm^{-1} at $\lambda \approx 729$ nm [38]), i.e. within the visible regime that extends up to 780 nm [41], one may find that the minimum 3 dB-optical-loss propagation distance is $x_{min} = \ln 2/g_{max} \approx 4.15\,\mu$m (at $\lambda \approx 729$ nm), and $x_{min}/a_{111} \approx 17$, where we have assumed a typical value of $a_{111} \approx 250$ nm [11]. Thus, even for wavelengths corresponding to the red section of the visible spectrum where clearly the absorption is large, we may still have appreciable penetration of the incident light inside the Si-based structure over several unit cells. Moreover, the effective free-carrier lifetime of photoexcited carriers inside the Si structure can be dramatically reduced by creating highly doped p+ and n+ regions at its (suitably designed) ends/edges and then reverse biasing the resulting p–i–n diode structure, similarly to the configurations used in [42]–[44]. The applied voltage will induce a strong electric field across the intrinsic Si DIOPC backbone, sweeping out the generated electron–hole pairs from the whole structure under reverse bias [42]–[44]. As a result, the absorption of light in the Si-based DIOPC will be further reduced and the optical response of the structure will be accordingly enhanced. The strong electric field inside

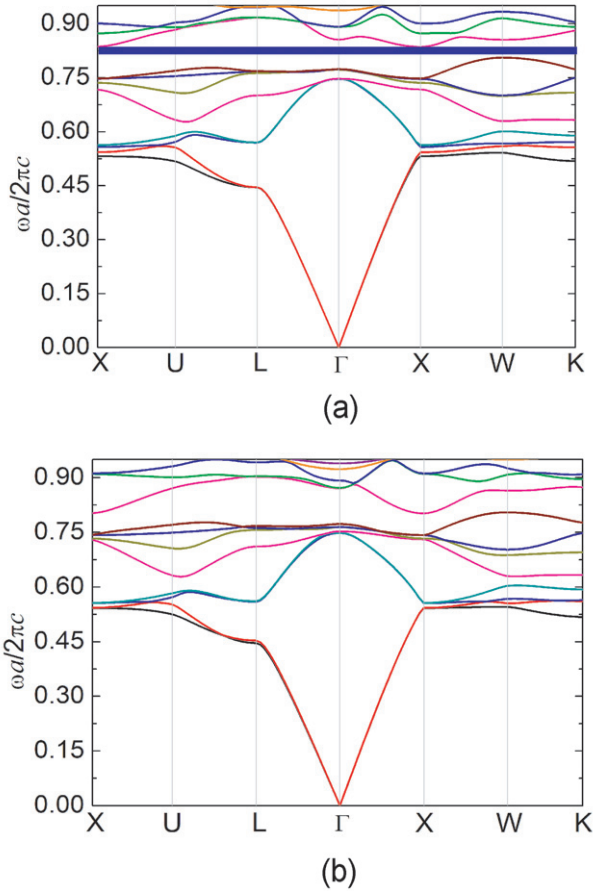

Figure 6. Band structure of the DIOPC, with the titania core spheres (a) being in their 'natural' (111) position and (b) shifted along the (100) direction. The silicon background has refractive index $n_{Si} = 3.736$. The core sphere and cylinder radii are chosen to be $0.18a$ and $0.126a$, respectively. The pore radius is $0.354a$.

the intrinsic backbone can, of course, also be used for collectively moving along its direction the spheres that reside inside the air pores of the DIOPC since, as we highlighted in section 2, these spheres contain subwavelength plasmonic cores, which are sensitive to external electric and/or magnetic fields.

The following simulations were, thus, performed using a purely real refractive index for the background material. Further, the herein Si-based DIOPC structure has additional cylindrical channels of radius R_{cyl}, interconnecting the air pores, as illustrated in figure 2(a), and the movable core spheres are made of titania ($n_{sp} = n_{TiO_2} = 2.54$).

Figure 6(a) illustrates the band diagram of the present DIOPC with the titania spheres being in their natural (111) position. For simplicity, the presence of the small inorganic (metallic) inclusions inside the core spheres is not taken into account in these calculations. The radii of the core, cylinder and air pores are, respectively, $R_{sp} = 0.18a$, $R_{cyl} = 0.126a$ and $R_p = 0.354a$. One can observe from figure 6(a) that a *complete* bandgap, highlighted by the black region, opens up between the eighth (brown) band at point W and the 9th (red) band at point X.

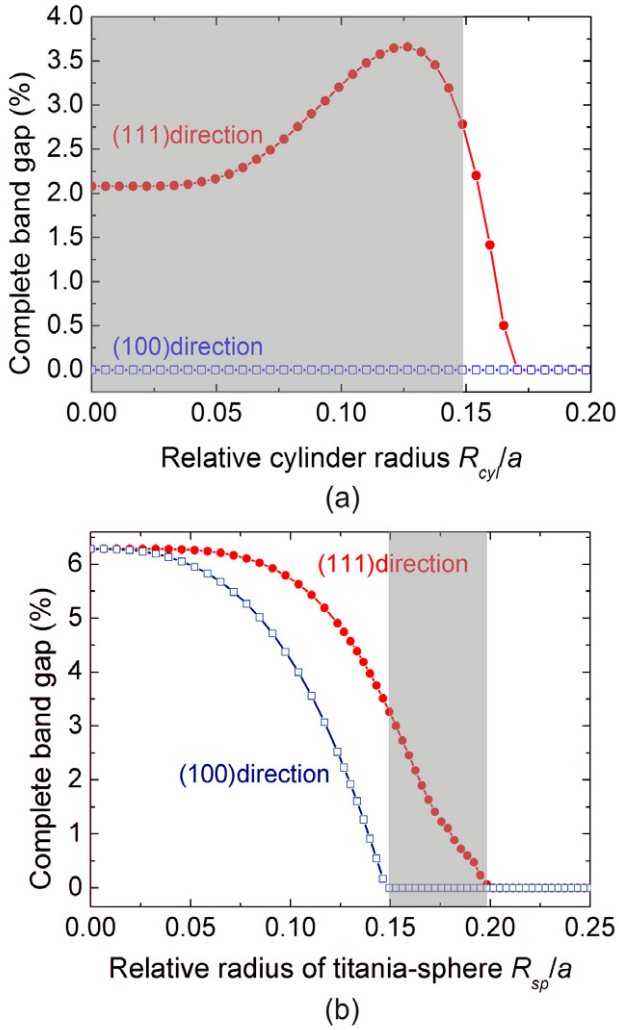

Figure 7. Variations of the complete bandgap for two switching states: spheres being in their 'natural' (111) position and shifted along the (100) direction. (a) Dependence of the bandgap size on R_{cyl}, for $R_{\mathrm{sp}} = 0.18a$. (b) Dependence of the bandgap size on R_{sp}, for $R_{\mathrm{cyl}} = 0.11a$. Parameter ranges in which a complete switching is experimentally feasible are highlighted by the gray shaded areas.

Since the upper edge of the PBG is limited by the X point of the 9th band, and we empirically know that the upper (air) bands are usually more susceptible to modifications in the refractive index distribution, we anticipate that shifting the titania spheres toward the (100) direction, which corresponds to the X point, should appreciably modify the shape of the 9th band at that point, and may result in the closing of the PBG [29]. Prompted by this observation, we shift the core spheres along (100) and calculate the resulting dispersion diagram. Figure 6(b) reports the result of such a calculation with all optogeometric parameters being those of figure 6(a). We note that the previously complete bandgap is here altogether closed, with the perturbation of the 9th band being particularly noticeable at point X, as expected. One may thus decidedly conclude that it is possible to completely open and close the PBG present in the

Si-based DIOPC, by suitable movement and/or positioning of the titania spheres inside the air pores of the structure.

Crucially, this scheme also allows for sizeable bandgap switching and, furthermore, it turns out to be very stable with respect to variations of R_{cyl} for the two switching states. The latter point is of great experimental interest since the control of R_{cyl} during the fabrication process is an important issue [11, 12]. Figure 7(a) displays the variations of the complete PBG with the relative radius of the cylinder R_{cyl}/a, for a core sphere radius $R_{sp} = 0.18a$. We infer from this figure that for this choice of R_{sp} switching of the complete PBG is, in principle, possible for the entire range of cylinder radii $0.0 \leqslant R_{cyl} \leqslant 0.170a$. The highlighted region indicates the experimentally interesting range of cylinder radii, since the maximum value that R_{cyl} can assume in practice has to be smaller than R_{sp}, in order for each titania sphere to be confined to its corresponding air pore and not fall through the cylinders. One can also observe that within the aforementioned range we never have formation of a complete PBG when the titania spheres are shifted in the (100) direction. As a result, the investigated switching mechanism can be completely independent of R_{cyl}, provided that R_{cyl} remains relatively small. It is also to be noted that within this range of cylinder radii the switchable PBG exceeds 2.26%, and assumes a maximum value of approximately 3.78%.

Finally, we studied the dependence of the complete PBG on the radius of the titania spheres, for fixed $R_{cyl} = 0.11a$, and present the results in figure 7(b). One may observe that the curve that is associated with the (100) shift of the spheres drops off faster compared with the curve that corresponds to the (111) shift. Accordingly, there is a region of sphere radii, $0.178a \leqslant R_{sp} \leqslant 0.221a$, highlighted by the gray zone in figure 7(b), wherein we can switch from a complete PBG when the spheres are shifted along (111), to a closed PBG when the spheres are shifted along (100). Within this range the maximum switchable PBG is a sizeable 3.76%.

4. Conclusions

In summary, we have presented a systematic investigation of the PBG switching capabilities of DCPC and DIOPC. Our analysis revealed that both classes of PC structures exhibit photonic stopgaps, which can be tuned by variations of the air pore radii. The DIOPC structure, further, has the potential for real-time switching of its optical properties, by collective movement of its core spheres in response to external magnetic or electric fields. Upon suitable optimization, this structure can also allow for a *complete* PBG switching, which turns out to be of the order of 3% and almost entirely independent of the radii of the interconnecting cylinders (which are difficult to control during the fabrication process). The present scheme may thus offer an elegant, conceptually simple and experimentally feasible route to photonic functionality at the telecommunication and the visible regime, which can be useful in the realization of iridescent surfaces, switchable windows and in the dynamic control of optical properties.

Acknowledgments

We thank P Spahn, C Jamois, K Boehringer and J Allam for fruitful discussions and J Hamm for technical assistance. This work was supported by the UK Engineering and Physical Sciences Research Council (EPSRC). KLT acknowledges support from the Royal Academy of Engineering and the EPSRC through a research fellowship.

References

[1] Pursiainen O L J, Baumberg J J, Winkler H, Viel B, Spahn P and Ruhl T 2007 *Opt. Express* **15** 9553
[2] Pursiainen O L J, Baumberg J J, Ryan K, Bauer J, Winkler H, Viel B and Ruhl T 2005 *Appl. Phys. Lett.* **87** 101902
[3] Rahman F and Johnson N P 2008 *Opt. Photonics News* **19** 24
[4] Rahman F and Rue R M De La 2007 *Photonics Spectra* **41** 52
[5] Iler R K 1965 *Nature* **207** 472
[6] Darragh P J, Gaskin A J, Terrell B C and Sanders J V 1966 *Nature* **209** 13
[7] Nishimura S, Abrams N, Lewis B A, Halaoui L I, Mallouk T E, Benkstein K D, van de Lagemaat J and Frank A J 2003 *J. Am. Chem. Soc.* **125** 6306
[8] Yablonovitch E 1987 *Phys. Rev. Lett.* **58** 2059
[9] John S 1987 *Phys. Rev. Lett.* **58** 2486
[10] Blanco A *et al* 2000 *Nature* **405** 437
[11] Ruhl T, Spahn P, Hermann C, Jamois C and Hess O 2006 *Adv. Funct. Mater.* **16** 885
[12] Ruhl T, Spahn P, Winkler H and Hellmann G P 2004 *Macromol. Chem. Phys.* **205** 1385
[13] Sumioka K, Kayashima H and Tsutsui T 2002 *Adv. Mater.* **14** 1284
[14] Busch K and John S 1998 *Phys. Rev.* E **58** 3896
[15] Foulger S H, Jiang P, Lattam A, Smith D W, Ballato J Jr, Dausch D E, Grego S and Stoner B R 2003 *Adv. Mater.* **15** 685
[16] Sheng P *et al* 2000 *Pure Appl. Chem.* **72** 309
[17] Gu Z Z, Fujishima A and Sato O 2000 *J. Am. Chem. Soc.* **122** 12387
[18] Leonard S W, Mondia J P, van Driel H M, Toader O, John S, Busch K, Birner A, Gösele U and Lehmann V 2000 *Phys. Rev.* B **61** R2389
[19] Takeda H and Yoshino K 2002 *J. Appl. Phys.* **92** 5658
[20] Schuller C, Klopf F, Reithmair J P, Kamp M and Forchel A 2003 *Appl. Phys. Lett.* **82** 2767
[21] Mertens G, Röder T, Matthias H, Harsmann H, Kitzerow H S, Schweizer S L, Jamois C, Wehrspohn R B and Neubert M 2003 *Appl. Phys. Lett.* **83** 3036
[22] Kubo S, Gu Z Z, Takahashi K, Fujishima A, Segawa S and Sato O 2004 *J. Am. Chem. Soc.* **126** 8314
[23] Leonard S W, van Driel H M, Schilling J and Wehrspohn R 2000 *Phys. Rev.* B **66** 161102
[24] Mazurenko D A, Kerst R, Dijkhuis J I, Akimov A V, Golubev V G, Kurdyukov D A, Pevtsov A B and Sel'kin A V 2003 *Phys. Rev. Lett.* **91** 213903
[25] Hu X, Zhang Q, Liu Y, Cheng B and Zhang D 2003 *Appl. Phys. Lett.* **83** 2518
[26] Becker C, Linden S, von Freymann G, Wegener M, Tétreault N, Vekris E, Kitaev V and Ozin G A 2005 *Appl. Phys. Lett.* **87** 091111
[27] Euser T G, Wei H, Kalkman J, Jun Y, Polman A, Norris D J and Vos W L 2007 *J. Appl. Phys.* **102** 053111
[28] Johnson P M, Koenderink A F and Vos W L 2002 *Phys. Rev.* B **66** 081102
[29] Aryal D P, Tsakmakidis K L, Jamois C and Hess O 2008 *Appl. Phys. Lett.* **92** 011109
[30] Aryal D P, Tsakmakidis K L and Hess O 2008 *Photonic crystals: From Fundamentals to Functional Photonic Materials* (Bellingham, WA: SPIE) chapter 8, at press
[31] Wijnhoven J E G J and Vos W L 1998 *Science* **281** 802
[32] Wijnhoven J E G J, Bechger L and Vos W L 2001 *Chem. Mater.* **13** 4486
[33] Palacios-Lidón E, Blanco A, Ibisate M, Meseguer F, López C and Sánchez-Dehesa J 2002 *Appl. Phys. Lett.* **81** 4925
[34] Li Z Y and Zhang Z Q 2000 *Phys. Rev.* B **62** 1516
[35] Johnson S G and Joannopoulos J D 2001 *Opt. Express* **8** 173
[36] Vlasov Y A, Bo X-Z, Sturm J C and Norris D J 2001 *Nature* **414** 289
[37] Reed G T and Knights A P 2008 *Silicon Photonics: The State of the Art* (Chichester: Wiley)

[38] Aspnes D E 1988 Optical functions of intrinsic Si: table of refractive index, extinction coefficient and absorption coefficient vs energy (0 to 400 eV) *Properties of Silicon (Electronics Materials Information Service Datareviews, Series No. 4)* ed T H Ning and C Hilsum (London: INSPEC) pp 72–9
[39] Palik E D 1985 *Handbook of Optical Constants of Solids* (London: Academic)
[40] Huang K C, Lidorikis E, Jiang X, Joannopoulos J D, Nelson K A, Bienstman P and Fan S 2004 *Phys. Rev.* B **69** 195111
[41] Shalaev V M 2007 *Nat. Photonics* **1** 41
[42] Xu Q, Schmidt B, Pradham S and Lipson M 2005 *Nature* **435** 325
[43] Rong H, Liu A, Jones R, Cohen O, Hak D, Nicolaescu R, Fang A and Paniccia M 2005 *Nature* **433** 292
[44] Chen H-T, Padilla W J, Zide J M O, Gossard A C, Taylor A J and Averitt R D 2006 *Nature* **444** 597